# Watching *Pseudomonas mevalonii* HMG-CoA Reductase in Action

*Himani N. Patel,[1] Vatsal Purohit,[2] Calvin N. Steussy,[2] Timothy Schmidt,[2] Paul Helquist,[1]*

*Cynthia V. Stauffacher,[2*] Olaf Wiest[1*]*

1 Department of Chemistry and Biochemistry, University of Notre Dame, IN 46556, USA

2 Department of Biological Sciences, Purdue University, West Lafayette, IN 47907, USA

## Introduction

Enzymes are the molecular machines of the cell that do the functional work necessary for living organisms. Their complex mechanisms employ changes across scales of structure from the assembly of large multi-macromolecular complexes to the orientation of specific amino acid residues around a substrate to enable reactivity or to exert control over a biological process. Structural and computational studies have assembled series of snapshots of enzymes in various substates of their reaction with the goal of examining the catalytic mechanisms over another scale, the time scale. Combining the strengths of computational dynamics and experimental time-resolved crystallography promises a more detailed understanding the atomistic details of an enzymatic reaction.

Deciphering an enzymatic mechanism is even more challenging for an enzyme that has multiple intermediates. Here, we study 3-hydroxy-3-methyl-glutaryl coenzyme A reductase (HMGR, Figure 1a,b) from *Pseudomonas* mevalonii, which is an oxidoreductase of the isoprenoid pathway that performs three reactions to interconvert a thioester, HMG-CoA, into a primary alcohol, mevalonate (or vice versa), using two cofactor molecules and producing two key intermediates, mevadehyde and mevaldyl-CoA (Figure 1). The complex mechanism of the reaction (Figure 1c) has been studied in detail experimentally[1-4] and computationally[4, 5] and has several features that make it suitable for the combined application of these methods to elucidate the

complete reaction pathway. The complex, multi-step reaction is reversible in bacterial HMG-CoA reductase such as the one from *Pseudomonas mevalonii* (PmHMGR) and is known to proceed in the crystal.[2] We recently demonstrated that the unusual pH profile of the reaction can be used to trigger it by a pH jump experiment.[6]

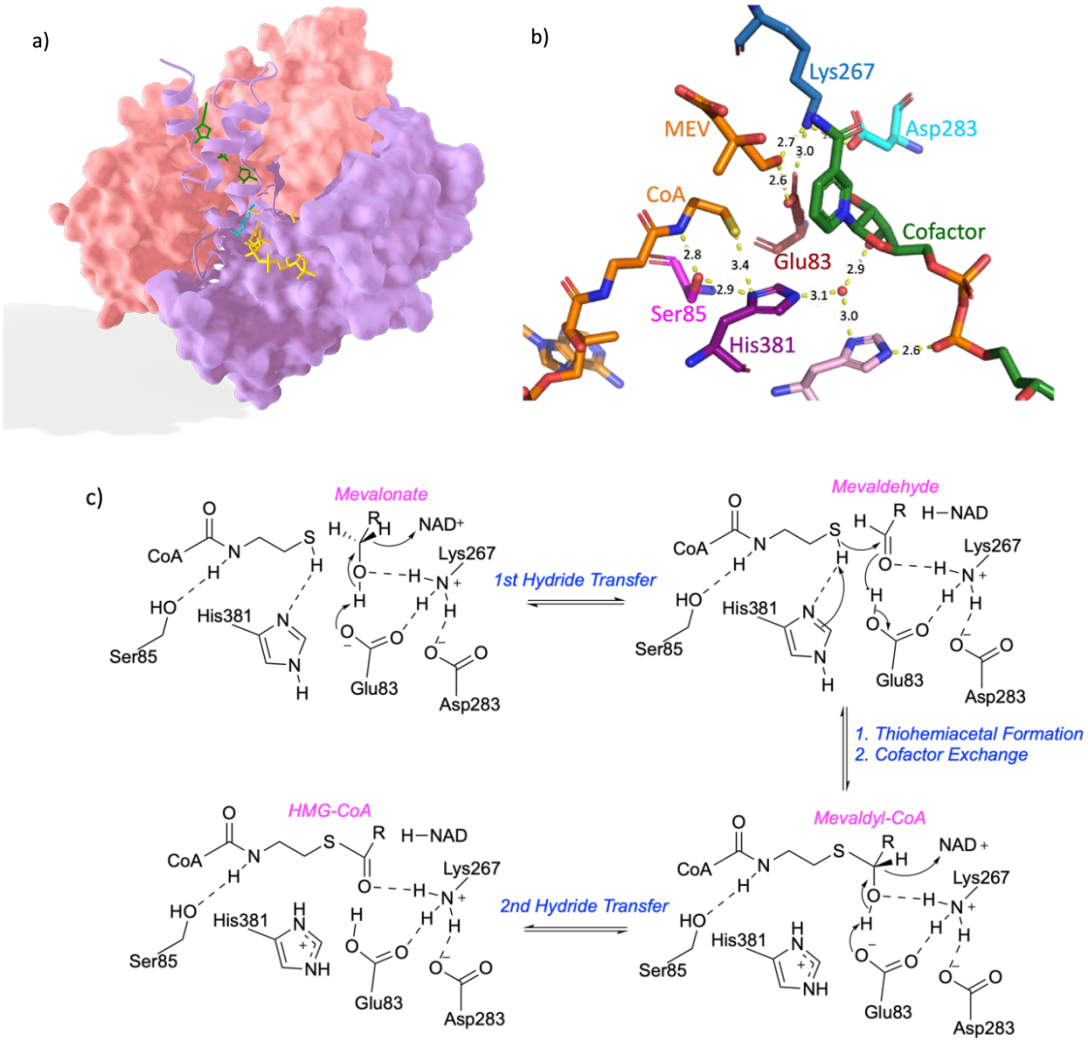


**Figure 1.** a) The homodimeric (pink and purple surface model) structure of PmHMGR bound to mevalonate, coenzyme A, and NAD+ (pdb code 9DCP, 2.06Å resolution). b) closeup of the active site. c) proposed reaction mechanism of PmHMGR[5]

In this study we have used time-resolved crystallography to observe reaction progression in an enzyme from a structural point of view, demonstrating that the reaction can run in the crystal and doing an initial evaluation of some of the subtle changes in the active site which lead to the formation of the thiohemiacetal. Among the variety of techniques that can be used to initiate and subsequently observe the progression of the enzymatic reaction we have chosen to use the pH jump mechanism we have developed that takes advantage of the pH reaction profile of PmHMGR.[6] Detailed observations of movements of the substrates and residues critical to the reaction mechanism as well as estimates of the extent of the reaction at various widely spaced time points have been made.

## Results & Discussion:

**Observing thiohemiacetal formation in *Pm*HMGR using time-resolved crystallography**: To compare changes in the thiohemiacetal bond region between mevalonate and CoA, we generated composite omit maps (Methods-Data Analysis), which provide the cleanest density maps for the HMGR ligands in the evolving reaction. These maps showed no density in the thiohemiacetal region during the first minute after reaction initiation, although the gap between the carbonyl carbon of the first intermediate, mevaldehyde, and the CoA sulfur was reduced. However, between 2 and 4 minutes, a significant buildup of thioester bond density was detected, indicating the formation of a thiohemiacetal at the enzyme's active site (Fig. 2). The data indicate that the appearance of the second reaction intermediate (mevaldyl-CoA) in *Pm*HMGR crystals requires several minutes under these experimental pH jump conditions.

These time-resolved observations confirm that catalysis by *Pm*HMGR does occur in the crystal and that we can observe one of the important steps in the reaction profile in detail over an experimentally accessible range of time steps.

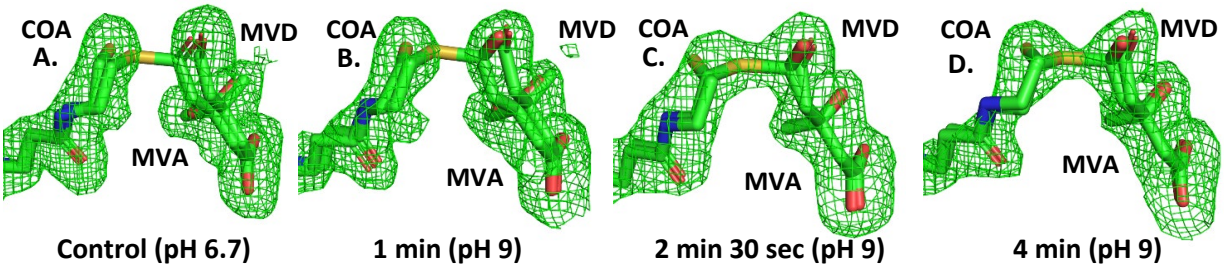


**Figure 2.** Changes in composite omit map density before (A) and after a pH-jump (B–D) in the thiohemiacetal region between mevaldehyde and CoA at the *Pm*HMGR active site. MVD – mevaldehyde; MVA – mevalonate; CoA – thiol end of extended CoA in the enzyme.

Since the composite omit map density still represents an average over the entire crystal, calculations were made to extract the combination of partial occupancies that would reflect the experimental electron density at any one time point. To evaluate changes in the populations of mevaldyl-CoA, mevaldehyde, and CoA upon initiation of a pH-jump, we compared 2Fo–Fc and Fo-Fc maps generated using varying occupancies for each ligand independently. By adjusting the selected occupancies, we optimized the combined density observed for mevaldyl-CoA, mevaldehyde, and CoA, ensuring that only 2Fo–Fc density was present without residual Fo–Fc difference density. This ensures that the occupancies of these molecules were now most optimally aligned with the time post-pH jump datasets of Figure 3.

Analyzing this data, in structures spanning from the pre pH-jump state (pH 6.7) to the post pH-jump state (pH 9) at 1 minute, no significant density was observed in the region between mevalonate and CoA across all tested combinations of occupancies. However, starting at 2 minutes and 20 seconds post pH-jump, a buildup of density for the thiohemiacetal region of mevaldyl-CoA became apparent at an occupancy of 0.4 for this intermediate (Figure 3). This density became more pronounced 4 minutes after reaction initiation, with an occupancy of 0.5 for mevaldyl-CoA. The

increasing occupancy and density for mevaldyl-CoA further indicate the formation of this intermediate *in crystallo*.

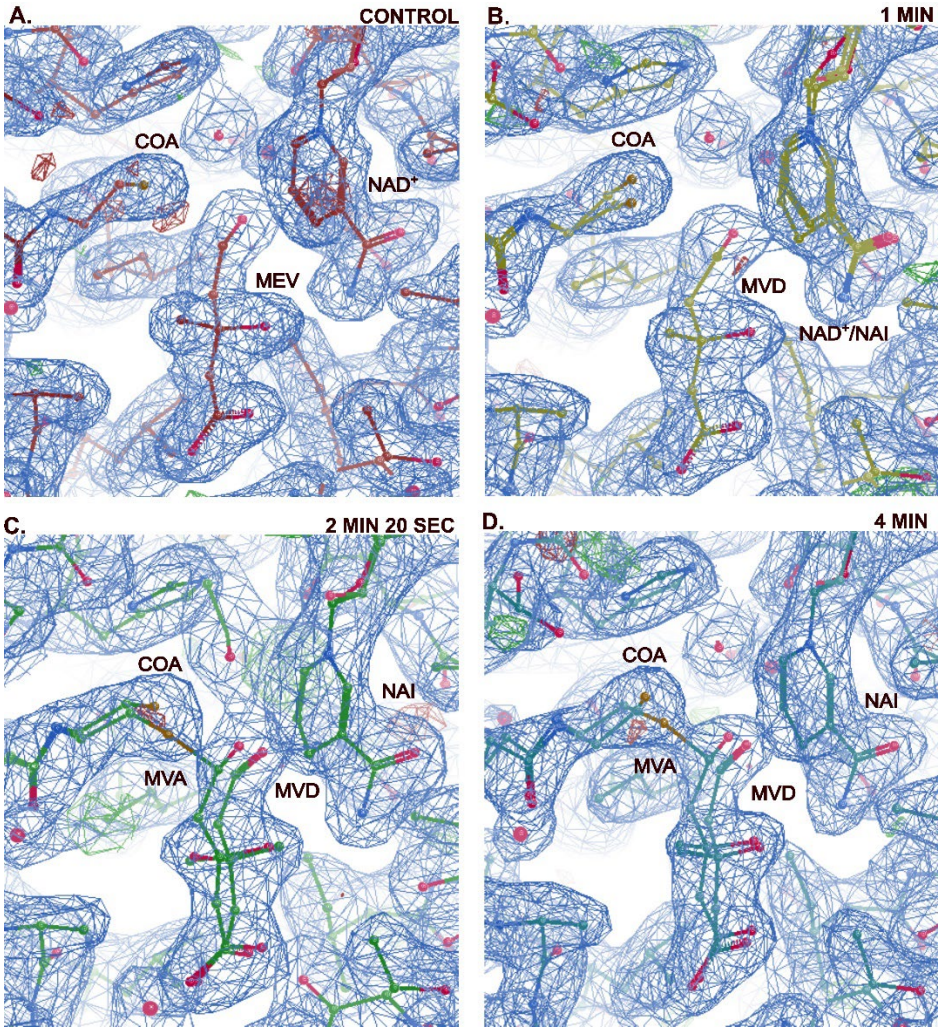


**Figure 3.** 2Fo–Fc density analysis at the *Pm*HMGR active site for thiohemiacetal formation. (A-B) Control (pdb 9DG2) and 1 minute post pH-jump (pdb 9DCP) show no observable thiohemiacetal density. (C) At 2 minutes 20 seconds (pdb 9DPG), thiohemiacetal density begins to appear, corresponding to an occupancy of 0.4. (D) At 4 minutes (pdb 9DY6), the density is more pronounced, with an occupancy of 0.5.

We then analyzed the changes in the active site region following reaction initiation, focussing on the point of formation of the thiohemiacetal bond. 1 minute after reaction initiation, the population of NADH, as measured by the occupancy of the cofactor, is higher (0.67) compared to NAD (0.29), suggesting a substantial population has undergone the hydride transfer step for this portion of the *Pm*HMGR reaction. Based on this observation, we modeled the first intermediate, mevaldehyde, in the active site in order to reflect the majority of the substrate components present. Then each of the following three time points past the pH jump were examined for significant structural changes required for thiohemiacetal formation.

For the pH jump at 1min we observed that the most significant change in active site arrangement relative to thiohemiacetal formation was a repositioning of CoA mediated by Ser 85. The distance between the Ser-O and CoA pantothenic acid N decreased by 0.45 Å (Figure 4C). This interaction appears to stabilize the strained configuration of CoA necessary for correct positioning for a hydride transfer to the thiohemiacetal in the following reaction step.[2] We also noted a more subtle movement of His 381 toward CoA at this point in the reaction, consistent with the proton transfer expected between the cosubstrate and the catalytic residue prior to thiohemiacetal formation (Figure 4B). The role of this reorientation will be discussed in more detail below.

At 2 minutes and 20 seconds, as thiohemiacetal density becomes apparent, the CoA thiol is observed to orient somewhat further toward an interaction with the terminal carbon of mevaldehyde (Figure 4A). The Ser 85 is now observed to be reorienting in its position rrelative to CoA, corresponding to the Ser(O)-CoA(N) modest distance increase of 0.6 Å (Figure 4C).

The Ser(O)-CoA(N) contact reaches its most favorable interaction configuration at 4 minutes, coinciding with the highest observed thiohemiacetal density at equal occupancy with CoA. Throughout this sequence of mechanistic steps, the active site Lys-Asp-Glu remains static, consistent with its role as the proton donor and oxyanion hole in this mechanism (Figure 1c)

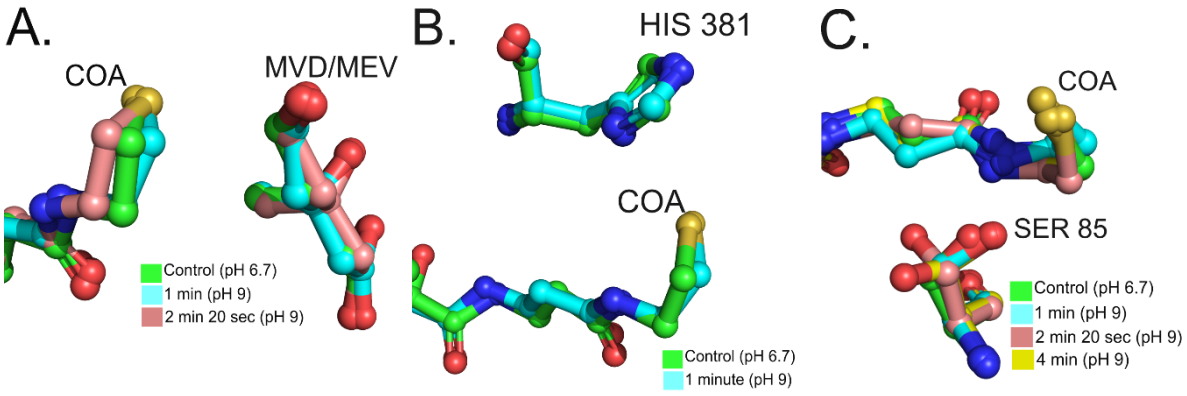


**Figure 4:** Structural changes in the active site after reaction initiation. *(A)* Repositioning of CoA in the active site over time, highlighting shifts in the pantothenic acid thiol regions. *(B)* Movement of His 381 toward CoA 1 minute after a pH-jump. (C) Positioning of SER 85 relative to CoA after the pH jump.

**Molecular dynamics studies** The availability of experimental structures close to the activated complex of the thiohemiacetal formation provides a new possibility to study the complex mechanism of HMG CoA reductase[5] in unprecedented detail using a combination of experimental and computational methods, a long-standing goal in our groups.[7, 8] Here, we focus on the role of His 381, which as shown in Figure 1 as a base in the proton transfers associated with the C-S bond formation. As shown in Figure 4B, the shift of His 381 is subtle and its protonation state cannot be ascertained from the 2Å structures in this series. In addition to the different possible protonation states, the neutral form of His 381 can also exist in two different states known as δ and ε protomers, but it is unclear from the crystal structures which one is more likely to be the base in the reaction. We therefore analyze 100 ns MD trajectories of different protonation states of the active site residues with particular emphasis on the interaction network of His 381.

Starting from the crystal structure at pH9 obtained before any C-S bond formation can be observed, different protomers of His 381 and the catalytic residue Glu$^{83}$ were considered. Using the nomenclature of the AMBER force fields, the three protomers HID, HIE and HIP of His 381 were considered the protonated Glu$^{83}$ (Figure 5c). Earlier QM/MM studies[9] indicate that the reaction barrier for the subsequent hydride transfer is lower for the neutral Glu 83 in agreement with the proposed reaction mechanism shown in Figure 1 that suggests a neutral Glu 83 for the thiohemiacetal formation.[5] Therefore, only the results for this protonation state are shown in Figure 5. We also studied different protomers His$^{385}$,[10] but only the ε-protomer is discussed in the context of this study.

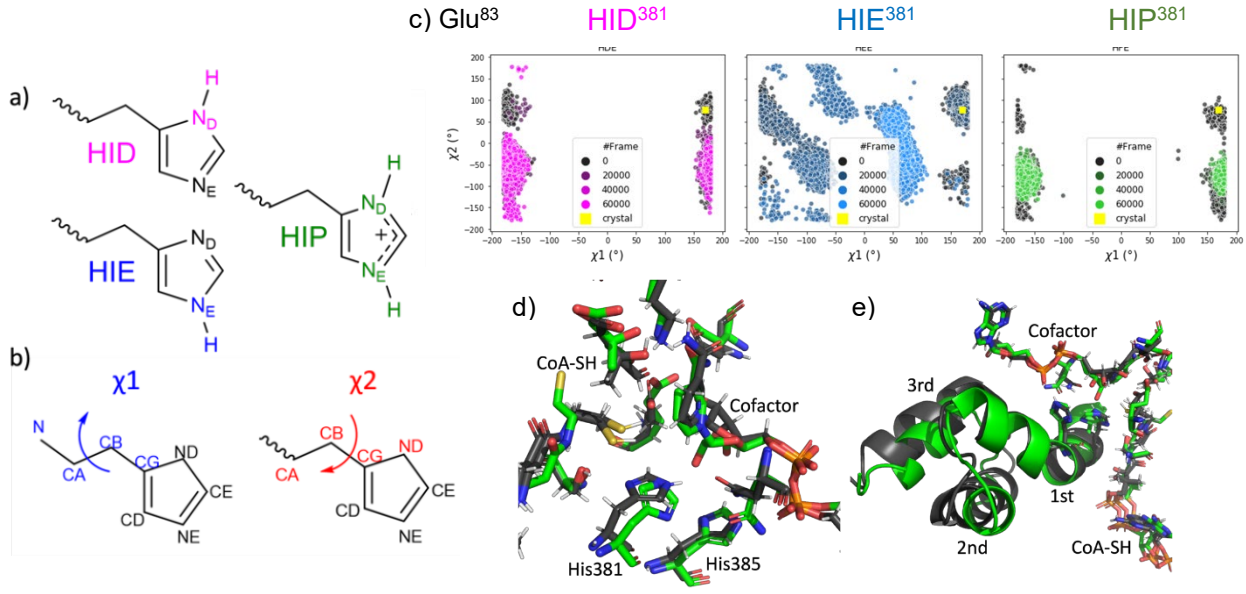


**Figure 5**. a) Three protonation states of histidine b) definition of dihedral angles, $\chi^1$ and $\chi^2$, of histidine, c) dihedral angles $\chi^1$ and $\chi^2$ of the three protomers of His 381 with Glu 83 protonated (c). Experimental value from the crystal structure is shown as a yellow square, d,e) Overlay of the structures of the active site and the flap domain helices from the crystal structure (colored) and the MD simulations (grey, average of the last 5000 frames of simulation) of the Glu 83/HIE 381 system.

Figure 5c shows the side chain conformers of His 381 for the three protomers. The HIE 381 protomer is distinct from the other two in that it allows the His 381 into the position required for deprotonation of the CoA thiol. This is shown in Figure 5d, where His 381 positions the unprotonated δ-nitrogen to act as the base even closer than in the crystal structure that served as the starting point for the MD simulation (shown in color in Figure 5 d,e). In comparison, the position of the remaining residues including the unusual, curved conformation of the first helix of the flap domain (Figure 5e) are maintained throughout the simulation.

In summary, this work demonstrates the applicability of the pH jump technique to observe the formation of the thiohemiacetal intermediate in the reaction catalyzed by HMG CoA reductase using time-resolved crystallography. These structures are close to the activated complex of the carbon-sulfur bond formation that also involves a deprotonation of the thiol. Molecular dynamics simulations show how the flexibility of key residues, specifically the role of His 381 as the base, are coupled to the experimentally observed bond formation. As the prediction of enzyme structures using artificial intelligence becomes more widely accepted, the combination of experimental and computational methods at or near the activated complex of a reaction as demonstrated here is the next logical step in the elucidation of complex enzyme mechanisms.

## Methods

### Time-resolved Crystallographic Data and Analysis

**Sample preparation:** *Pm*HMGR for this study was expressed, purified, and crystallized using previously established methods.[11] Crystals of the size 0.3-0.4 nm were utilized for time-resolved measurements and cryoprotected in 32 % glycerol prior to any soaking steps. The experiment was designed to sample at fairly large time intervals the first step of the reaction in Figure 1c ("1st

Hydride Transfer"). To produce *in crystallo* intermediates, we utilized the pH-jump method. The crystal environment was slowly exchanged with a 1.2 M ammonium acetate, 100 mM ADA and 32 % PEG-400 (pH 6.7) environment using a soaking time of 8 hours.[6] The ligands mevalonate, CoA and $NAD^+$ were then introduced at a 5 mM, 1 mM and 1 mM concentration respectively for a period of 4 hours to ensure sufficient binding. The crystals were then transferred to a pH 9 environment for different time periods ranging from 1 to 4 minutes before being freeze-trapped in liquid nitrogen.

**Data collection:** Diffraction data for *Pm*HMGR crystals was obtained at the Advanced Photon Source at Argonne National Laboratory, Sector 23-ID-B and 23-ID-D. A wavelength of 1.033 Å was used to obtain diffraction data using either an Dectris Eiger-16 M or Dectris Pilatus 3-6 M detector. Crystals with a diffraction quality of 1.99 – 2.5 Å were obtained.

**Data Analysis:** All the datasets were indexed using the HKL2000 suite.[12] The space group of all the structures was found to be $I4_132$. A mevalonate, CoA and $NAD^+$ bound structure of *Pm*HMGR was used to determine a molecular replacement solution of all the structures using the CCP4 suite.[13] The structures were refined without any ligands bound at the enzyme active site using a rigid body refinement, followed by a simulated annealing and successive real-space refinements.[14-16] The ligands NADH, $NAD^+$, mevalonate and CoA were added using the program Ligandfit.[17, 18] The ligands mevaldyl-CoA and mevaldehyde were added using the HIC-UP server to provide a starting set of coordinates. Mevaldyl-CoA was placed in the structure by using a previously obtained thiohemiacetal bound structure (PDB) and doing a LSQ mainchain atom alignment. The geometry and energy parameters of the ligand models were corrected based on the atomic resolution, small molecule structures available through the Cambridge Small Molecule Database. Subsequent refinements were done on the obtained structures in the presence of ligands until their $R_{free}$ and $R_{work}$ values reached their minima. The program Molprobity[19] was used to make

corrections for Ramachandran and rotamer outliers and for bonds and angles. Polder maps and simulated annealing maps generated using the phenix polder map and 'composite omit map' programs were used to determine changes in the electron density of the nicotinamide ring to determine NADH production and evolution of the thioester bond in post pH-jump structures.[20, 21] The data collection statistics are in the table below (Table 1).

**Table 1.** Crystallographic Data and Refinement Statistics for Structures Collected Pre and Post pH-Jump at Various Time Intervals with *Pm*HMGR Crystals

| | PRE pH-jump (pH-jump buffer, pH 6.7) | 1 minute pH9 | 2 minutes 20 seconds pH 9 | 4 minutes pH 9 |
|---|---|---|---|---|
| PDB Entry | 9DG2 | 9DCP | 9DPG | 9DY6 |
| Wavelength | 1.033 | 1.033 | 1.033 | 1.033 |
| Resolution range | 46.1 - 1.93Å | 44.3 - 2.06 Å | 43.9 - 2.50 Å | 46.0 - 2.25 Å |
| Space group | I4(1)3 2 | I4(1)3 2 | I4(1)3 2 | I4(1)3 2 |
| a,b,c (Å) | 225.67 | 225.77 | 224.16 | 225.48 |
| α=β=γ (deg) | 90 | 90 | 90 | 90 |
| Unique reflections | 139577 | 115085 | 62768 | 87895 |
| Multiplicity | 10.4 (9.4) | 16.2 (11.6) | 5.0 (4.4) | 5.0 (5.0) |
| Completeness (%) | 85.82 (1.52) | 89.88 (9.23) | 98.08 (81.33) | 98.69 (84.40) |
| Mean I/sigma(I) | 9.33 (0.49) | 9.88 (0.34) | 10.01 (1.47) | 9.90 (1.21) |
| Wilson B-factor | 20.16 | 26.57 | 34.21 | 29.85 |
| R-merge | 31.33 | 32.04 | 13.1 | 12.82 |
| CC1/2 | 0.989 (0.125) | 0.994 (0.105) | 0.994 (0.529) | 0.995 (0.453) |
| CC* | 0.997 (0.472) | 0.998 (0.437) | 0.998 (0.832) | 0.999 (0.79) |
| R-work (%) | 17.84 | 21.39 | 18.95 | 18.41 |
| R-free (%) | 21.71 | 24.17 | 23.87 | 22.68 |
| Protein residues | 795 | 802 | 793 | 800 |
| RMS(bonds) | 0.01 | 0.009 | 0.003 | 0.004 |
| RMS(angles) | 0.98 | 0.81 | 0.65 | 0.76 |
| Ramachandran favored (%) | 96.7 | 96.87 | 96.7 | 96.4 |
| Ramachandran allowed (%) | 3.05 | 3.13 | 3.3 | 3.6 |
| Ramachandran outliers (%) | 0 | 0 | 0 | 0 |
| Rotamer outliers (%) | 0 | 0.17 | 0 | 0 |
| Clashscore | 3.16 | 3.13 | 3.63 | 2.95 |
| Average B-factor | 25.53 | 39.68 | 38.39 | 40.44 |
| macromolecules | 24.93 | 39.65 | 38.25 | 40.06 |
| Ligands | 33.76 | 39.93 | 45.79 | 54.88 |
| Solvent | 31.38 | 40.13 | 34.63 | 39.77 |

**Determining changes in intermediate populations with an occupancy analysis:**

To compare the populations of different intermediates in post-reaction *Pm*HMGR structures following a pH-jump, we performed B-factor refinements for each structure at varying occupancies (ranging from 0.0 to 1.0) for the intermediates mevaldehyde and CoA, as well as the reaction intermediate mevaldyl-CoA. By analyzing changes in the 2Fo–Fc and Fo–Fc maps, we identified the predominant intermediate present in each structure obtained after reaction initiation. The occupancy was set to the value at which no observable Fo–Fc density remained and only 2Fo–Fc density was present, indicating agreement with the structure. The final structures were subsequently refined at the locked occupancy.

**MD simulations** The crystal structure (resolution 2.10Å) obtained from the pH-jump experiments,[22] 20 seconds after initiating the oxidative reaction, at pH 9 and bound to cofactor (NAD+ or NADH), mevaldehyde, and coenzyme A, was used in this computational study. The residue of interest, His 381 (purple stick model in Figure 1b), is on the first helix of the flap domain close to His385 (pink stick model in Figure 1b). The protonation state of His385 was also studied since it would influence the non-covalent interactions around His 381.

These models were prepared for molecular dynamics simulation using Amber18.[23] All systems had $NAD^+$, CoA, and mevaldehyde as ligands. Amber ff14SB, the general amber force field (GAFF), and published $NAD^+$ parameters were used for the protein, mevaldehyde, and cofactor, respectively.[24-27] Partial charges for mevaldehyde were obtained using the RESP protocol[28, 29] calculated at the B3LYP/6-31G** level of theory in Gaussian16.[30] The systems were solvated using the TIP3P water model and neutralized using sodium ions.[31, 32] Minimization was performed over four cycles with weak positional restraints (10 kcal/mol.Å) on the protein followed by heating to 300 K in six increments of 50 K. A brief equilibration is performed at constant

volume and 300K temperature for 20 ps before equilibrating the system at constant temperature (300 K) using Langevin thermostat and pressure, maintained at 1 atm using Berendsen barostat, for 200 ps. Finally, the production run was performed at an NPT ensemble for 100 ns with a 2 fs time step (input coordinate and topology files in SI). All analyses were performed using *cpptraj*.[33]

The analysis of these systems focused on selecting a single protonation state for His385 in order to study the protonation state of His 381 in subsequent simulations. Determining the protonation state of His 381 would assist in rationalizing the pH dependence of the oxidative reaction in *Pm*HMGR.

After deciding on the most likely protonation state of His385 from the studies described above, a second set of systems vary the protonation states of Glu83 and His 381. Glu83 was also investigated since it is an ionizable catalytic residue that is close to His 381. Previous computational studies have shown the preference for a neutral Glu83 with a positively charged His 381 (HIP).[9]

**Acknowledgements:** We gratefully acknowledge support by the National Institute of Health through grant (R01GM111645) to C.V.S., P.H. and O.W and a CBBI fellowship to H.N.P. (training grant T32GM075762). Data collection was done on beamlines at GM/CA@APS, funded by the National Cancer Institute (ACB-12002) and the National Institute of General Medical Sciences (AGM-12006, P30GM138396). The Eiger 16M detector at GM/CA-XSD was funded by NIH grant S10 OD012289. This research used resources of the Advanced Photon Source, a U.S. Department of Energy (DOE) Office of Science User Facility operated for the DOE Office of Science by Argonne National Laboratory under Contract No. DE-AC02-06CH11357."

## References


1. Lawrence, C. M.; Rodwell, V. W.; Stauffacher, C. V., Crystal structure of Pseudomonas mevalonii HMG-CoA reductase at 3.0 angstrom resolution. *Science* **1995,** *268*, 1758-1762.

2. Steussy, C. N.; Critchelow, C. J.; Schmidt, T.; Min, J.-K.; Wrensford, L. V.; Burgner, J. W.; Rodwell, V. W.; Stauffacher, C. V., A Novel Role for Coenzyme A during Hydride Transfer in 3-Hydroxy-3-methylglutaryl-coenzyme A Reductase. *Biochemistry* **2013,** *52*, 5195-5205.

3. Tabernero, L.; Bochar, D. A.; Rodwell, V. W.; Stauffacher, C. V., Substrate-induced closure of the flap domain in the ternary complex structures provides insights into the mechanism of catalysis by 3-hydroxy-3-methylglutaryl-CoA reductase. *Proc. Natl. Acad. Sci USA* **1999,** *96*, 7167-71.

4. Hedl, M.; Tabernero, L.; Stauffacher, C. V.; Rodwell, V. W., Class II 3-Hydroxy-3-Methylglutaryl Coenzyme A Reductases. *J. Bact.* **2004,** *186*, 1927-1932.

5. Haines, B. E.; Wiest, O.; Stauffacher, C. V., The Increasingly Complex Mechanism of HMG-CoA Reductase. *Acc. Chem. Res.* **2013,** *46*, 2416-2426.

6. Purohit, V.; Steussy, C. N.; Rosales, A. R.; Critchelow, C. J.; Schmidt, T.; Helquist, P.; Wiest, O.; Mesecar, A.; Cohen, A. E.; Stauffacher, C. V., pH-dependent reaction triggering in PmHMGR crystals for time-resolved crystallography. *Biophys J* **2024,** *123*, 622-637.

7. Quinn, T. R.; Steussy, C. N.; Haines, B. E.; Lei, J.; Wang, W.; Sheong, F. K.; Stauffacher, C. V.; Huang, X.; Norrby, P. O.; Helquist, P.; Wiest, O., Microsecond timescale MD simulations at the transition state of Pm HMGR predict remote allosteric residues. *Chem. Sci.* **2021,** *12*, 6413-6418.

8. O'Connell, R. J.; Dolphin, N. J.; Ferraudi, G.; Lee, M.; Stauffacher, C. V.; Helquist, P.; Wiest, O., Synthesis of Caged HMG-CoA Reductase Substrates for the Elucidation of Cellular Pathways. *J. Org. Chem.* **2024,** *89*, 18739–18745.

9. Haines, B. E.; Steussy, C. N.; Stauffacher, C. V.; Wiest, O., Molecular modeling of the reaction pathway and hydride transfer reactions of HMG-CoA reductase. *Biochemistry* **2012,** *51*, 7983-7995.

10. Patel, H. N. Computational Studies on HMG-CoA Reductases and other biomolecular systems. University of Notre Dame, 2023.

11. Jordan-Starck, T.; Rodwell, V., Pseudomonas mevalonii 3-hydroxy-3-methylglutaryl-CoA reductase: Characterization and chemical modification. *J. Biol. Chem.* **1989,** *264*, 17913-17918.

12. Otwinowski, Z.; Minor, W., Processing of X-ray diffraction data collected in oscillation mode. *Methods Enzymol* **1997,** *276*, 307-26.

13. Winn, M. D.; Ballard, C. C.; Cowtan, K. D.; Dodson, E. J.; Emsley, P.; Evans, P. R.; Keegan, R. M.; Krissinel, E. B.; Leslie, A. G.; McCoy, A.; McNicholas, S. J.; Murshudov, G. N.; Pannu, N. S.; Potterton, E. A.; Powell, H. R.; Read, R. J.; Vagin, A.; Wilson, K. S., Overview of the CCP4 suite and current developments. *Acta Cryst. D Struct Biol* **2011,** *67*, 235-242.

14. Murshudov, G. N.; Skubak, P.; Lebedev, A. A.; Pannu, N. S.; Steiner, R. A.; Nicholls, R. A.; Winn, M. D.; Long, F.; Vagin, A. A., REFMAC5 for the refinement of macromolecular crystal structures. *Acta Cryst. D Struct Biol* **2011,** *67*, 355-367.

15. Murshudov, G. N.; Vagin, A. A.; Dodson, E. J., Refinement of macromolecular structures by the maximum-likelihood method. *Acta Cryst. D Struct Biol* **1997,** *53*, 240-255.

16. Afonine, P. V.; Grosse-Kunstleve, R. W.; Echols, N.; Headd, J. J.; Moriarty, N. W.; Mustyakimov, M.; Terwilliger, T. C.; Urzhumtsev, A.; Zwart, P. H.; Adams, P. D., Towards automated crystallographic structure refinement with phenix.refine. *Acta Crystallogr D Biol Crystallogr* **2012,** *68*, 352-367.

17. Terwilliger, T. C.; Klei, H.; Adams, P. D.; Moriarty, N. W.; Cohn, J. D., Automated ligand fitting by core-fragment fitting and extension into density. *Acta Cryst. D Struct Biol* **2006,** *62*, 915-922.

18. Terwilliger, T. C.; Adams, P. D.; Moriarty, N. W.; Cohn, J. D., Ligand identification using electron-density map correlations. *Acta Cryst. D Struct Biol* **2007,** *63*, 101-107.

19. Williams, C. J.; Headd, J. J.; Moriarty, N. W.; Prisant, M. G.; Videau, L. L.; Deis, L. N.; Verma, V.; Keedy, D. A.; Hintze, B. J.; Chen, V. B.; Jain, S.; Lewis, S. M.; Arendall, W. B., 3rd; Snoeyink, J.; Adams, P. D.; Lovell, S. C.; Richardson, J. S.; Richardson, D. C., MolProbity: More and better reference data for improved all-atom structure validation. *Protein Sci* **2018,** *27*, 293-315.

20. Liebschner, D.; Afonine, P. V.; Moriarty, N. W.; Poon, B. K.; Sobolev, O. V.; Terwilliger, T. C.; Adams, P. D., Polder maps: improving OMIT maps by excluding bulk solvent. *Acta Cryst. D Struct Biol* **2017**, 148-157.

21. Terwilliger, T. C.; Grosse-Kunstleve, R. W.; Afonine, P. V.; Moriarty, N. W.; Adams, P. D.; Read, R. J.; Zwart, P. H.; Hung, L.-W., Iterative-build OMIT maps: map improvement by iterative model building and refinement without model bias. *Acta Cryst. D Struct Biol* **2008,** *64*, 515-524.

22. Purohit, V. Elucidating the HMG-CoA Reductase Reaction Mechanism using pH-Triggered Time-Resolved X-Ray PhD Thesis. Purdue University 2021.

23. Case, D. A.; Ben- Shalom, I. Y.; Brozell, S. R.; Cerutti, D. S.; Cheatham Iii, T. E.; Cruzeiro, V. W. D.; Darden, T. A.; Duke, R. E.; Ghoreishi, M. K.; Gilson, M. K.; Gohlke, A. W.; Goetz, A. W.; Greene, D.; Harris, R.; Homeyer, N.; Izadi, S.; Kovalenko, A.; Kurtzman, T.; Lee, T. S.; LeGrand, S.; Li, P.; Lin, C.; Liu, J.; Luchko, T.; Luo, R.; Mermelstein, D. J.; Merz, K. M.; Miao, Y.; Monard, G.; Nguyen, C.; Nguyen, H.; Omelyan, I.; Onufriev, A.; Pan, F.; Qi, R.; Roe, D. R.; Roitberg, A.; Sagui, C.; Schott-Verdugo, S.; Shen, J.; Simmerling, C. L.; Smith, J.; Salomon-Ferrer, R.; Swails, J.; Walker, R. C.; Wang, J.; Wei, H.; Wolf, R. M.; Wu, X.; Xiao, L.; York, D. M.; Kollman, P. A., AMBER18. **2018**.

24. Maier, J. A.; Martinez, C.; Kasavajhala, K.; Wickstrom, L.; Hauser, K. E.; Simmerling, C., ff14SB: Improving the Accuracy of Protein Side Chain and Backbone Parameters from ff99SB. *J. Chem. Theor. Comp.* **2015,** *11*, 3696-3713.

25. Pavelites, J. J.; Gao, J.; Bash, P. A.; Mackerell, A. D., A molecular mechanics force field for NAD+, NADH, and the pyrophosphate groups of nucleotides. *J. Comp. Chem.* **1997,** *18*, 221-239.

26. Wang, J.; Wang, W.; Kollman, P. A.; Case, D. A., Automatic atom type and bond type perception in molecular mechanical calculations. *J. Mol. Graph. Mod.* **2006,** *25*, 247-260.

27. Wang, J.; Wolf, R. M.; Caldwell, J. W.; Kollman, P. A.; Case, D. A., Development and testing of a general amber force field. *J. Comp. Chem.* **2004,** *25*, 1157-1174.

28. Wang, J.; Cieplak, P.; Kollman, P. A., How Well Does a Restrained Electrostatic Potential (RESP) Model Perform in Calculating Conformational Energies of Organic and Biological Molecules? *J. Comp. Chem.* **2000,** *21*, 1049-1074.

29. Bayly, C. I.; Cieplak, P.; Cornell, W. D.; Kollman, P. A., A Well-Behaved Electrostatic Potential Based Method Using Charge Restraints for Deriving Atomic Charges: The RESP Model. *J. Phys. Chem* **1993,** *97*, 10269-10280.

30. Frisch, M. J.; Trucks, G. W.; Schlegel, H. B.; Scuseria, G. E.; Robb, M. A.; Cheeseman, J. R.; Scalmani, G.; Barone, V.; Petersson, G. A.; Nakatsuji, H.; Li, X.; Caricato, M.; Marenich, A. V.; Bloino, J.; Janesko, B. G.; Gomperts, R.; Mennucci, B.; Hratchian, H. P.; Ortiz, J. V.; Izmaylov, A. F.; Sonnenberg, J. L.; Williams-Young, D.; Ding, F.; Lipparini, F.; Egidi, F.; Goings, J.; Peng, B.; Petrone, A.; Henderson, T.; Ranasinghe, D.; Zakrzewski, V. G.; Gao, J.; Rega, N.; Zheng, G.; Liang, W.; Hada, M.; Ehara, M.; Toyota, K.; Fukuda, R.; Hasegawa, J.; Ishida, M.; Nakajima, T.; Honda, Y.; Kitao, O.; Nakai, H.; Vreven, T.; Throssell, K.; Montgomery, J. J. A.; Peralta, J. E.; Ogliaro, F.; Bearpark, M. J.; Heyd, J. J.; Brothers, E. N.; Kudin, K. N.; Staroverov, V. N.; Keith, T. A.; Kobayashi, R.; Normand, J.; Raghavachari, K.; Rendell, A. P.; Burant, J. C.; Iyengar, S. S.; Tomasi, J.; Cossi, M.; Millam, J. M.; Klene, M.; Adamo, C.; Cammi, R.; Ochterski, J. W.; Martin, R. L.; Morokuma, K.; Farkas, O.; Foresman, J. B.; Fox, D. J. *Gaussian 16 Revision C.01*, Wallinford, CT, 2016.

31. Li, P.; Song, L. F.; Merz, K. M., Systematic parameterization of monovalent ions employing the nonbonded model. *J. Chem. Theor. Comp.* **2015,** *11*, 1645-1657.

32. Jorgensen, W. L.; Chandrasekhar, J.; Madura, J. D., Comparison of simple potential functions for simulating liquid water. *J. Chem. Phys.* **1983,** *79*, 926-935.

33. Roe, D. R.; Cheatham, T. E., PTRAJ and CPPTRAJ: Software for Processing and Analysis of Molecular Dynamics Trajectory Data. *J. Chem. Theor. Comp.* **2013,** *9*, 3084-3095.